Available online at www.sciencedirect.com
ScienceDirect
Earth and Planetary Science Letters 264 (2007) 226–244
EPSL
www.elsevier.com/locate/epsl

Density distribution of the India plate beneath the Tibetan plateau: Geophysical and petrological constraints on the kinetics of lower-crustal eclogitization

György Hetényi [a,*], Rodolphe Cattin [a], Fabrice Brunet [a], Laurent Bollinger [b], Jérôme Vergne [a], John L. Nábělek [c], Michel Diament [d]

[a] *Laboratoire de Géologie, Ecole Normale Supérieure, CNRS - UMR 8538, 24 rue Lhomond, 75005 Paris, France*
[b] *Laboratoire de Détection et de Géophysique, CEA, BP12, 91680 Bruyères-le-Châtel, France*
[c] *College of Oceanic and Atmospheric Sciences, Oregon State University, Corvallis OR 97331, USA*
[d] *Institut de Physique du Globe de Paris, 4 place Jussieu, 75252 Paris, France*

Received 22 May 2007; received in revised form 14 September 2007; accepted 25 September 2007
Available online 6 October 2007
Editor: C.P. Jaupart

Abstract

We combine seismological and Bouguer anomaly data with thermo-kinematic and petrological modelling to constrain the extent and kinetics of the eclogitization process in the Indian lower crust underthrusting Tibet. Based on Airy-type isostasy gravity modelling, we show that the presence of denser material (eclogites) is required beneath the Tibetan Plateau. Using the geometries of main crustal interfaces constrained by seismological experiments along three profiles perpendicular to the Himalayan arc, multilayer density-models suggest that eclogitization of the Indian lower crust is completed where the maximal depth of its descent is reached.

In an integrated geophysical and petrological approach, the temperature field of the studied area is determined and realistic pressure–temperature–density grids are calculated assuming different hydration levels for the Indian lower crust. The derived density profiles are used to forward model Bouguer anomalies and to compare them to the observations. It appears that eclogitization of the Indian lower crust is delayed compared to where it is expected to occur from phase equilibria. The results show that neither dry nor fully hydrated (free water in excess) lower-crust models are satisfactory. A hydration level of ca. 1 wt.% H_2O, consistent with a lower crust having experienced amphibolitic conditions, is more realistic and yields better results. On this basis, the densification delay of the Indian lower crust can be accounted for by a kinetical hindrance (overstepping) of the consumption of the plagioclase component (garnet and clinopyroxene forming reactions), which does not release water. Densification proceeds relatively rapidly (within 6 My) at higher pressure and temperature (at least 100 °C above equilibrium), when dehydration reactions start releasing water.

These results emphasize the key role of free water in metamorphic reaction kinetics and, consequently, on geodynamical processes.

Keywords: Bouguer anomaly; eclogite; metamorphic reaction kinetics; water; Tibet; India plate

* Corresponding author. Tel.: +33 1 44 32 22 50, +33 1 44 32 22 61; fax: +33 1 44 32 20 00.
E-mail address: hetenyi@geologie.ens.fr (G. Hetényi).

0012-821X/$ - see front matter © 2007 Elsevier B.V. All rights reserved.
doi:10.1016/j.epsl.2007.09.036

1. Introduction

The southern border of the Tibetan Plateau is the scene of continental collision since 50 Ma (Patriat and Achache, 1984). Over the last three decades this region has been extensively studied to understand both its building and its structure from various methods, including structural geology, petrologic observations, thermochronological data, GPS measurements and seismological experiments (*e.g.* Le Fort, 1986; Zhao et al., 1993; Jackson and Bilham, 1994; Lavé and Avouac, 2000; Bollinger et al., 2004; Bettinelli et al., 2006). The convergence across the Himalayas is mainly accommodated along major thrust faults, including the Main Central Thrust, the Main Boundary Thrust and the Main Frontal Thrust (Fig. 1) (*e.g.* Cattin and Avouac, 2000; Avouac, 2003). They all root to the Main Himalayan Thrust, which is imaged by the INDEPTH experiment between Sikkim and Lhasa (Nelson et al., 1996; Hauck et al., 1998) and by the Hi-CLIMB experiment in Central Nepal (Vergne et al., 2005). Indian crustal material is brought along this detachment to depths exceeding 50 km and at temperatures greater than 500 °C. In these pressure–temperature conditions major metamorphic reactions take place in the Indian lower crust (ILC). Previous studies have shown that eclogitization of the lower crust is a key process in the support of high topographic elevation of both Himalayas and Tibet (Bousquet et al., 1997; Henry et al., 1997; Cattin et al., 2001; Tiwari et al., 2006).

However, the pressure–temperature path of the underthrust lower crust is still poorly constrained. Based

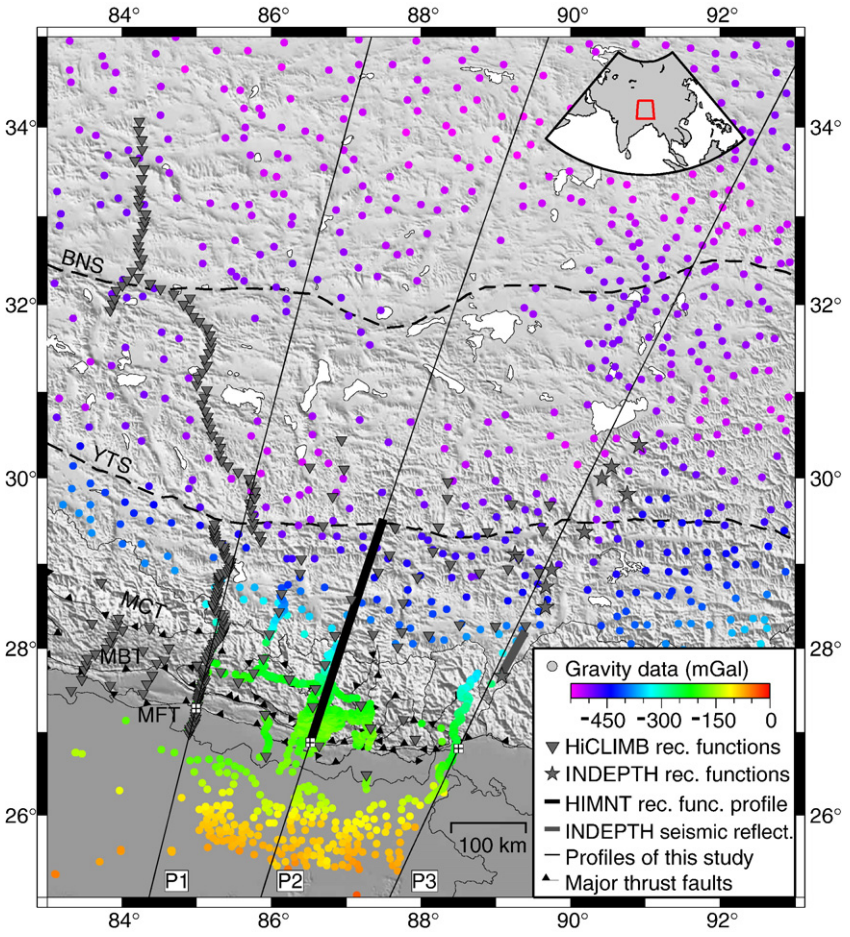

Fig. 1. Topographic map showing the area of interest, the location of the compiled seismological and gravity data, and the profiles used in this study. The crosses indicate the origin of profiles with the following co-ordinates and orientations: P1 (27.2829°N, 84.9885°E, N14°E); P2 (26.873°N, 86.517°E, N17.8°E); and P3 (26.8°N, 88.5°E, N25°E). YTS and BNS are the approximate locations of the Yarlung Tsangpo Suture and the Banggong-Nujiang Suture, respectively. MCT, MBT and MFT are the Main Central, Boundary and Frontal Thrusts, respectively. Data points less than 100 km away from each profile are projected and constitute the constraints on the depth of crustal structures as well as the gravity anomalies to fit for each profile. Topography data are from the SRTM30 database (Rodriguez et al., 2005). All depths in this study are referenced to sea-level.

on a receiver function profile and observed fast lower-crustal P-wave velocities, Schulte-Pelkum et al. (2005) argue that the lower crust is partially (~30%) eclogitized just South of the Yarlung Tsangpo Suture (YTS), and that the eclogitization process is governed by water availability. This implies that the lower-crustal material reaches the eclogite facies via granulite facies conditions, as shown in Le Pichon et al. (1997) for geotherms established after more than ~20 My of relaxation. However the latter study also shows that the geotherm may follow an amphibolite–eclogite and even a blueschist–eclogite path for shorter relaxation times between ~10–20 My and less than ~10 My, respectively.

The major shortcoming of these previous studies is the lack of accurate crustal geometries and thicknesses. Here we take advantage of the recent Hi-CLIMB seismic experiment, which imaged the main lithospheric structures from the Siwaliks to Central Tibet (Nábělek et al., 2005; Hetényi et al., 2006). Along with the INDEPTH and the HIMNT experiments (Zhao et al., 1993; Schulte-Pelkum et al., 2005), these seismological profiles crossing the southern border of the Tibetan Plateau are used with gravity data to study both lateral variations and eclogitization of the Indian lower crust. First we discuss the compensation of Tibetan Plateau in term of Airy isostasy. Next, using both gravity anomalies and geometrical constraints we estimate density variation in the India lower crust. To better constrain the P–T path of the Indian lower crust, we calculate density distributions from thermo-kinematic modelling and accurate petrogenetic grids. These modellings yield a multitude of density distributions, which we evaluate by comparing their synthetic gravity anomalies to observed ones. Finally, introduction of reaction kinetics to the model is appraised and interpreted, together with the path of the Indian lower crust in the pressure–temperature space.

2. Seismological and gravity anomaly datasets

Previous studies have used seismological or gravity observations to image the main structures of the Himalayas and Southern Tibet. The HIMNT experiment (Schulte-Pelkum et al., 2005) reveals a descending Moho beneath the Himalayas and its flattening South of the YTS, which is the northern extent of surface occurrences of Indian-affinity rocks. However, the Moho's geometry further North remains unknown because the YTS marks the northern extension of this experiment. More recently the Hi-CLIMB project gave a higher-resolution crustal image from the Ganges Basin to the North of the Banggong-Nujiang Suture (BNS) along ~85°E (Nábělek et al., 2005; Hetényi et al., 2006). Along this profile the descent of the India plate is clearly visible. The Indian lower crust smoothly crosses the YTS at depth, and underthrusts the southern part of the Tibetan Plateau almost until the BNS. This suture is known to be a major lithospheric limit: South of the BNS (Lhasa block), the crust is thicker and colder (Owens and Zandt, 1997), and shows better refracted wave propagation properties (Barazangi and Ni, 1982; Ni and Barazangi, 1983) than to its North (Qiangtang block). Analysis of Bouguer anomalies in the southern border of and across Tibet (Lyon-Caen and Molnar, 1983; Jin et al., 1996) shows gravity anomalies as low as −500 mGal (1 mGal$=10^{-5}$ m s^{-2}) and confirms a thickened crust all over the plateau.

To achieve good spatial coverage and study lateral variations on the southern border of the Tibetan Plateau, we gathered seismological and gravity anomaly data from several sources along three profiles associated with the INDEPTH, HIMNT and Hi-CLIMB seismological experiments (Figs. 1 and 2).

2.1. Seismological data

The seismological data come from three major experiments (Fig. 1). Phase 1 (South) of the Hi-CLIMB main array defines the line of profile P1 (Nábělek et al., 2005). Profile P2 passes along the HIMNT experiment line (Schulte-Pelkum et al., 2005). The southern path of the INDEPTH experiment through the Himalayas defines profile P3 (Nelson et al., 1996; Hauck et al., 1998). The obtained geometries of the main crustal boundaries are compared on Fig. 2.

The depth-constraints of crustal interfaces for the Hi-CLIMB experiment (triangles on Fig. 1) come from receiver function calculations. We computed the receiver functions using the iterative time-domain deconvolution method of Ligorría and Ammon (1999) using a band-pass filter between 0.01 Hz and 0.5 Hz corner frequencies and 100 iterations. Along the main array, the calculated receiver functions are migrated using the Common Conversion Point method (Zhu, 2000), including altitude corrections and with a 2-D velocity-model constrained by calculating average V_P/V_S-ratios using multiples (Nábělek et al., 2005). Using the P-to-S conversion image along with the stacked images of the multiples, we pick the depth of the Moho. The top of the Indian lower crust is well imaged beneath Southern Tibet (Lhasa block). It is located 15 km above the Moho and exhibits a seismic signature generally stronger than that of the Moho, indicating a major increase in density and velocity. This 15 km lower crust is present beneath the Indian shield, but its upper limit

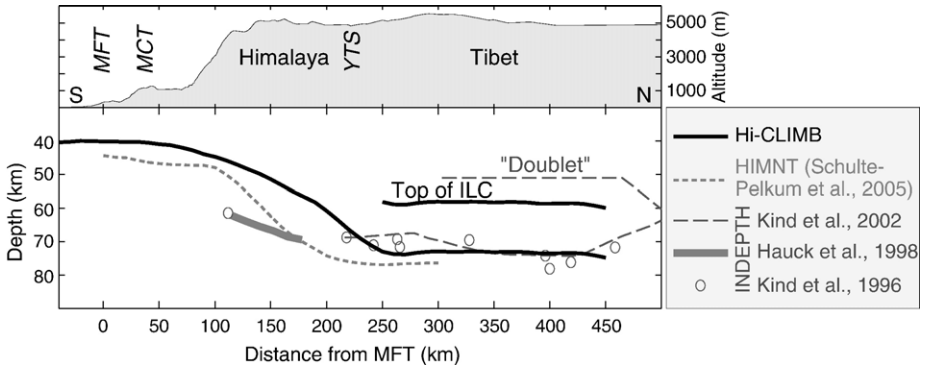

Fig. 2. Above: mean topography along profile P1. Below: geometry of the Moho constrained by three seismological experiments along profiles P1 (Hi-CLIMB), P2 (HIMNT) and P3 (INDEPTH). The top of the Indian lower crust (ILC) imaged along profile P1, and the equivalent "doublet" along profile P3, are also represented. Vertical exaggeration is 3:1.

has a smaller impedance contrast. For the lateral stations in Tibet (to the east of the main array), the depth of the Moho and its error-bar are estimated by using the H–κ stacking method (Zhu and Kanamori, 2000), and verified on sections migrated similarly as above.

The depth of the Moho along profile P2 comes directly from the interpretation of a migrated receiver function image of the HIMNT experiment (Schulte-Pelkum et al., 2005). We report this as the Moho depth, and use our interpretation of the HIMNT raw migration image (located at a little shallower depth) as an estimate for the error-bar.

The geometry of the Moho along profile P3 comes from several interpretations of the INDEPTH dataset. First, we use the Moho depth interpreted from the INDEPTH I and II seismic reflection profile (Hauck et al., 1998). We also use ten broadband stations (stars on Fig. 1) where the depth of the Moho has been estimated by individual receiver function inversions (Kind et al., 1996). On the migrated receiver function profile by Kind et al. (2002), one can note a double seismic discontinuity at ~55 km and ~70–75 km depth, similarly to what is observed in the Hi-CLIMB experiment (see above). Again, we interpret this double discontinuity as the contour of the underthrust Indian lower crust; its disappearance occurs close to the BNS and marks a transition toward the North where the entire lithosphere is of Eurasian affinity.

2.2. Bouguer anomaly data

The gravity data used in this study are compiled from four sources. The largest dataset comes from the International Gravimetric Bureau (Bureau Gravimétrique International, BGI, http://bgi.cnes.fr). These gravity data are gathered from different experiments, and are provided as processed Bouguer anomalies covering well India and Southern Nepal. Three arc-perpendicular profiles in Nepal were measured by joint French experiments (Cattin et al., 2001; Martelet et al., 2001). The eastern and the western of these profiles closely follow profiles P1 and P2, respectively. A study by Tiwari et al. (2006) provides new gravity data across the Sikkim Himalayas, which is in the continuation of the INDEPTH line corresponding to profile P3. Finally, we add the 5×5 *arcmin* gridded Bouguer anomalies over China (Sun, 1989), resampled at the locations of the measurements to overcome the smoothing processes. All these Bouguer anomalies were calculated using a reduction density of 2670 kg m^{-3}, and all datasets except BGI include terrain corrections up to 167 km (Cattin et al., 2001).

As gravity surveys yield relative measurements only, shifting of different datasets is allowed and required in order to obtain a homogeneous compilation. We use the BGI dataset as the reference, and check the consistency of the other datasets by comparing values at geographically close measurements, and by looking at profiles perpendicular to the Himalayas containing data from several datasets. The data by Tiwari et al. (2006) need to be shifted by −66 mGal; the data by Cattin et al. (2001) and Sun (1989) are consistent with the BGI reference.

The gravity data projected along the three 2000 km long profiles give similar trends with a ~500 mGal Bouguer anomaly decrease from the Ganges plain to the Tibetan Plateau. The average deviation on this general trend is on the order of ±10 mGal, with some smaller regions showing greater deviations of ±50 mGal.

3. Forward modelling: the isostatic case

The support of the Tibetan Plateau is often associated with crustal thickening in terms of local Airy isostasy

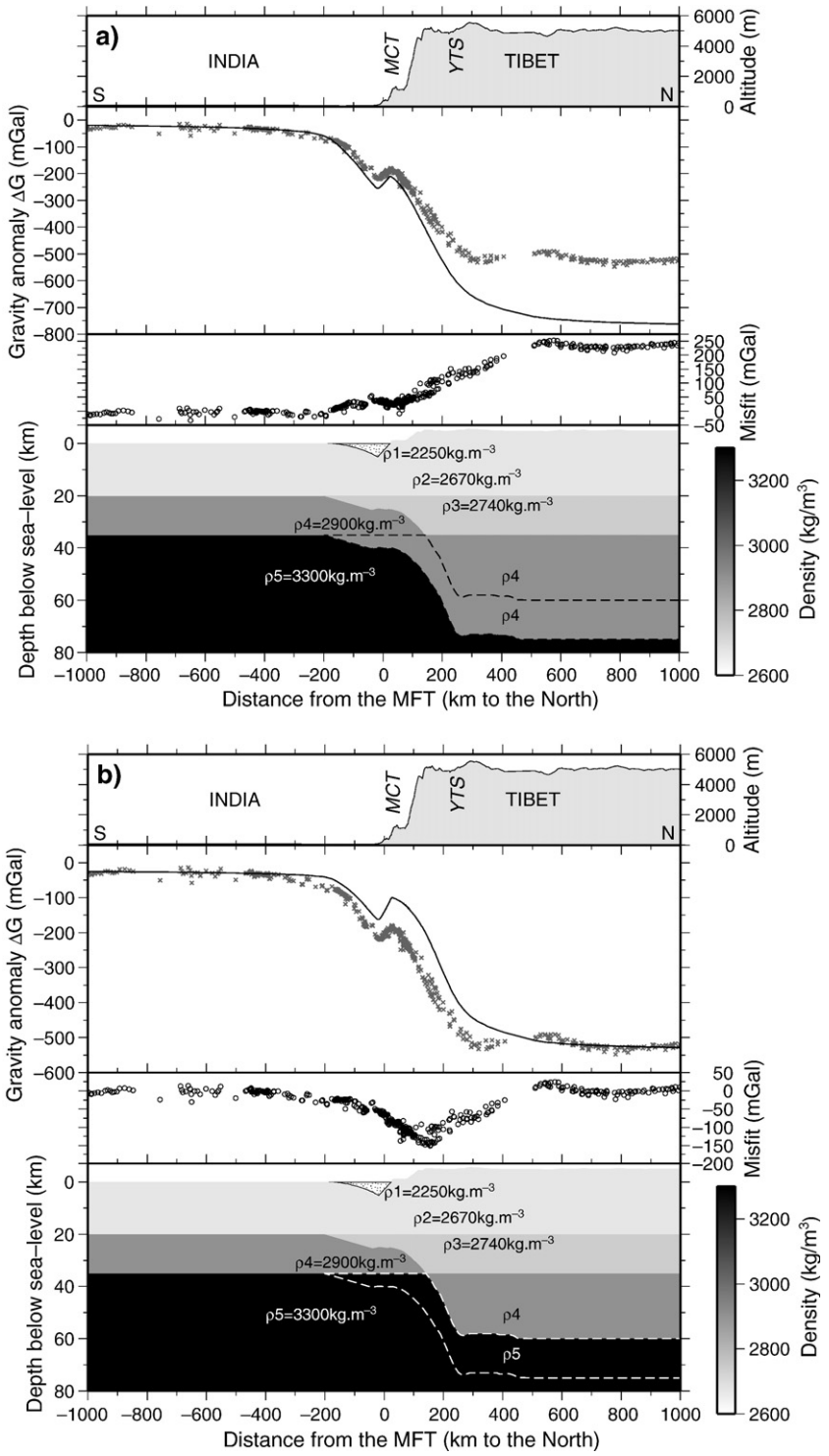

Fig. 3. Two end-member tests without and with densification of the Indian lower crust. Top: topography. Below: observed (crosses) and calculated (solid line) Bouguer anomalies along the profile, and their difference (below). Bottom: geometry and density of the bodies. The dashed line contours the underthrust ILC. (a) Model 1: no density variation within the Indian lower crust: while the differences between the model and the observations are small along most of the Southern part of the profile, a clear divergence appears north of 100 km. (b) Model 2: sudden density increase of the entire Indian lower crust beneath 35 km depth: the misfit is small on both ends of the profile, but there is a clear difference between −200 and 500 km.

(*e.g.* Jin et al., 1996; Cattin et al., 2001). Here we test this assumption using both gravity measurements and variations of crustal thickness inferred from seismological constraints along profile P1, where the best resolved and longest continuous dataset is available.

3.1. Calculations

Our method to calculate the 2D synthetic gravity anomalies is the following. First, we define the shape of the Moho on each profile from the seismological data described above. Based on observations along the Hi-CLIMB profile, where the Indian lower crust underthrusts the entire Lhasa block, we fix the lower-crustal thickness to 15 km. Similar value is used in the study of Tiwari et al. (2006), and is observed on INDEPTH data along profile P3. The Moho and the top of the Indian lower crust separate the model into three areas, to which we associate reference densities: ρ_M for the mantle, ρ_{LC} for the ILC, and ρ_{UC} for the upper crust. The model is extended at both ends: to the North at a constant depth corresponding to the northernmost observations, and to the South at 35 km Moho depth, as observed beneath the Indian shield (*e.g.* Saul et al., 2000). Finally, our approach includes a sedimentary domain corresponding to the foreland basin, with a density of $\rho_S = 2250$ kg m^{-3} and a geometry of the basement following Hetényi et al. (2006) for profiles P1 and P2 and Tiwari et al. (2006) for profile P3.

Then we use the algorithm of Won and Bevis (1987), based on the method of Talwani et al. (1959), to calculate the gravitational attraction of the defined polygons at the altitude of the observed data locations. The obtained anomaly curve is then shifted to the same level as the observations in the southern part of the profile, where the mean level of the gravity anomalies does not differ significantly from zero.

We estimate the sensitivity of our modelling by vertically shifting the Moho depth beneath Tibet by ±3 km, which is the average error-bar on the seismological image. The greatest deviation is ±49 mGal, which is the same magnitude as the misfit between modelled and observed anomalies, and as the maximum extent of data dispersion along the profile.

3.2. Constraints on isostasy

In order to explain the observed gravity anomalies, we first test models assuming local isostatic compensation (Airy, 1855) of the Tibetan plateau (the zone located beyond 300 km north of the MFT). These tests are performed using the topography and gravity data along profile P1, and with the simplification that the entire crust has a uniform density ($\rho_C = \rho_{LC} = \rho_{UC}$). In this case, the crustal root R (the deepening of the Moho) derives simply from topography as:

$$R = \frac{T \cdot \rho_C}{\Delta\rho}, \tag{1}$$

where $\Delta\rho = \rho_M - \rho_C$ is the density contrast across the Moho, and T is the average topography. Then the agreement of the observed (Obs_i) and calculated (Cal_i) gravity data is measured by the misfit function

$$\chi^2 = \frac{\sum_i^N ((\mathrm{Obs}_i - \mathrm{Cal}_i)/\sigma_i)^2}{N}, \tag{2}$$

where N is the number of data samples, and σ is an estimate of data dispersion, defined in 40 equidistant intervals along the entire profile as half of the difference between the highest and lowest data value.

The value of the misfit, calculated for a wide range of ρ_C and $\Delta\rho$, shows that local isostatic compensation would occur if the density of the crust and the mantle were low (2500 kg m^{-3} and 2800–3100 kg m^{-3}, respectively). Even though the density contrast across the Moho is consistent with previous studies (Jin et al., 1996; Cattin et al., 2001), the absolute values of density are inconsistent with those known for a typical mantle and an average crust (*e.g.* Turcotte and Schubert, 1982; Christensen and Mooney, 1995; Szafián and Horváth, 2006). Thus we conclude that the observed Bouguer anomalies are not compatible with a simple isostatic model, and that the primary density contrast beneath Tibet should be introduced at shallower depth. In order to explain the anomalies, we construct more realistic density models (see the next section), in which the used geometries already take into account regional isostatic effects due to the weight of the Tibetan plateau and the flexure of the India plate (Hetényi et al., 2006).

4. Density variations beneath Tibet

To better approach the real composition of the lithosphere, we take into account the density variations of the Indian lower crust due to eclogitization (see *e.g.* Henry et al., 1997, Cattin et al., 2001). In this metamorphic transformation process, the density of the lower crust increases to reach a value that is close to that of the mantle (Bousquet et al., 1997; Jull and Kelemen, 2001). Bousquet et al. (1997) determined simplified petrogenetic grids, which show that the density of eclogites depends on the initial composition of the rock as well as

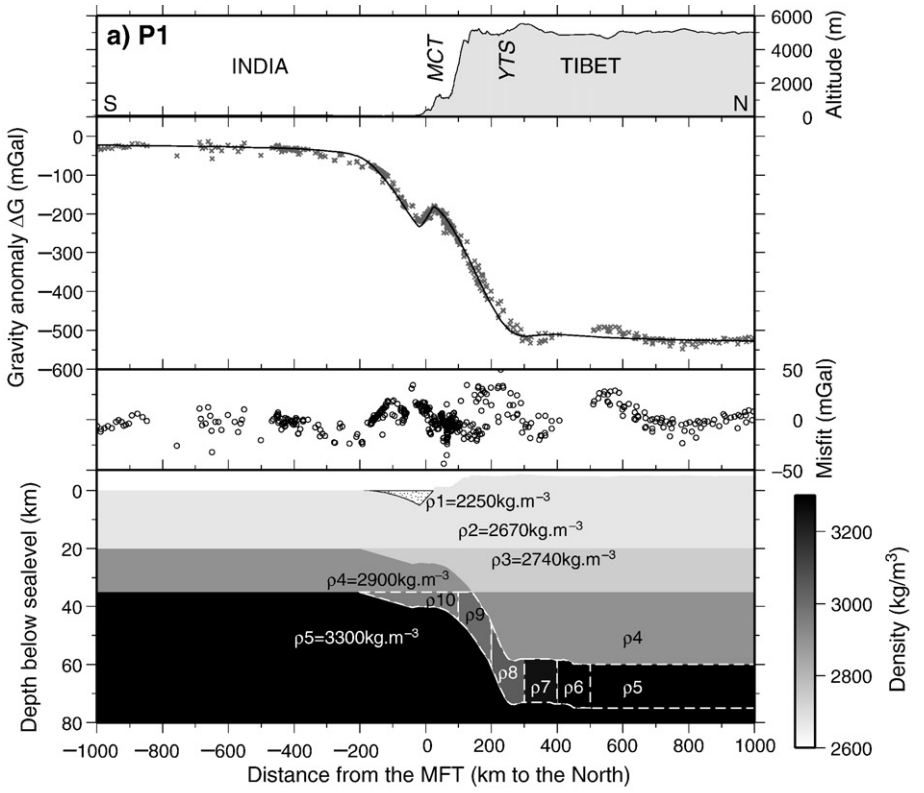
a) P1
INDIA
MCT
YTS
TIBET
S
N
Altitude (m)
Gravity anomaly ΔG (mGal)
Misfit (mGal)
Depth below sealevel (km)
ρ1=2250kg.m−3
ρ2=2670kg.m−3
ρ3=2740kg.m−3
ρ4=2900kg.m−3
ρ10
ρ9
ρ5=3300kg.m−3
ρ4
ρ8
ρ7
ρ6
ρ5
Density (kg/m3)
Distance from the MFT (km to the North)

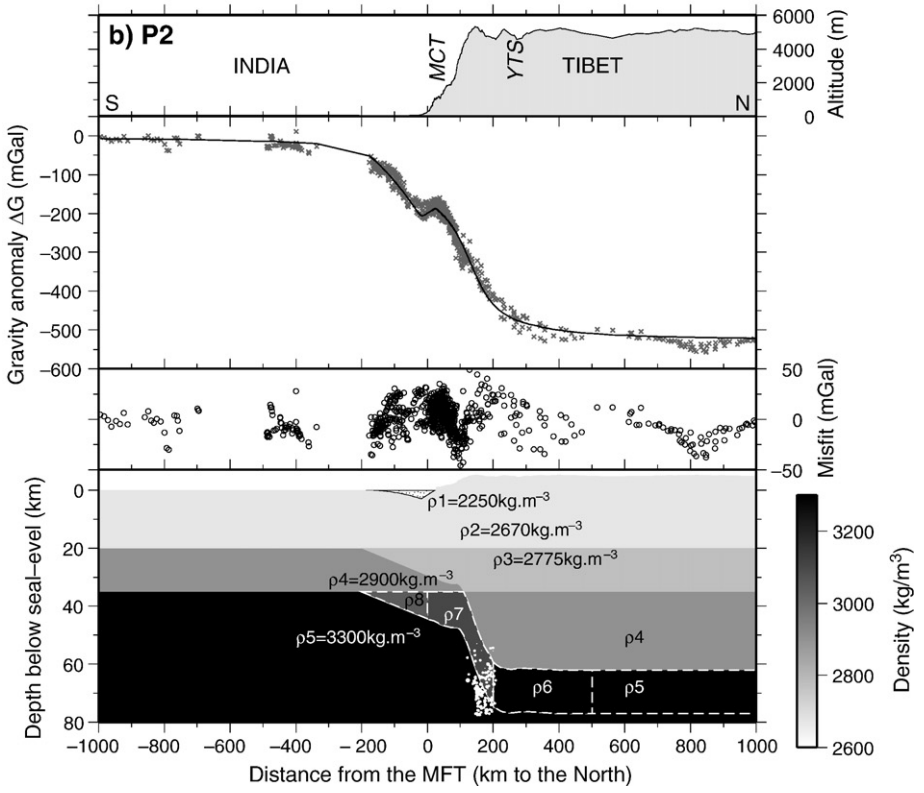
b) P2
INDIA
MCT
YTS
TIBET
S
N
Altitude (m)
Gravity anomaly ΔG (mGal)
Misfit (mGal)
Depth below seal–evel (km)
ρ1=2250kg.m−3
ρ2=2670kg.m−3
ρ3=2775kg.m−3
ρ4=2900kg.m−3
ρ8
ρ7
ρ5=3300kg.m−3
ρ4
ρ6
ρ5
Density (kg/m3)
Distance from the MFT (km to the North)

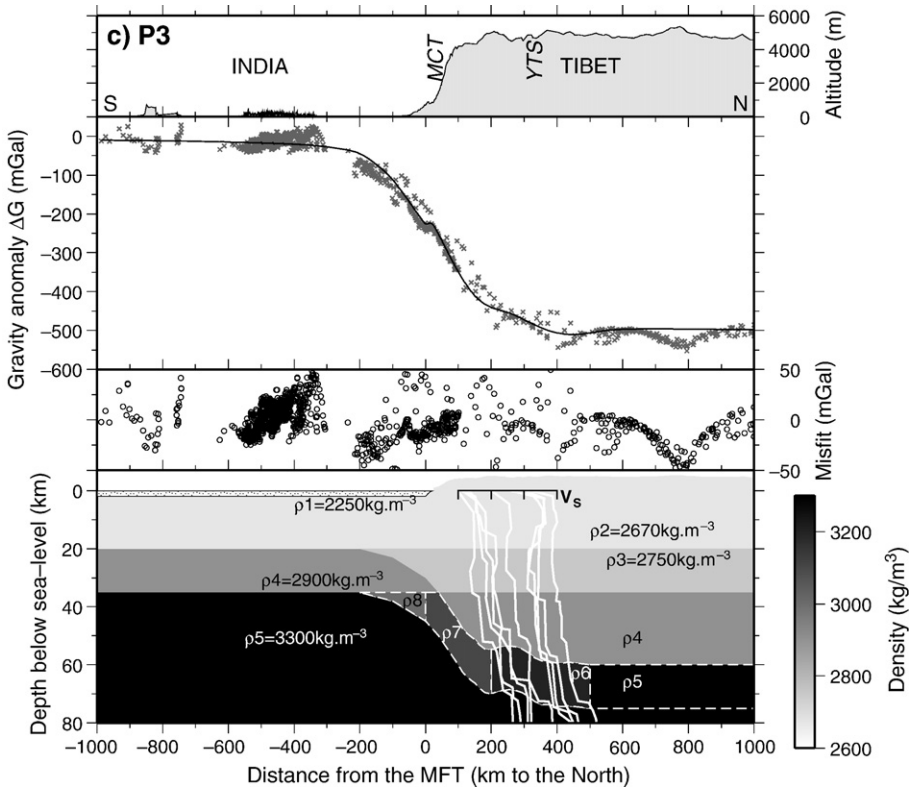

Fig. 4 (a)–(c) Three models corresponding to the best fit solutions at profiles P1, P2 and P3 (graphs as on Fig. 3). The imaged geometry of the Moho is assumed for all profiles with an Indian lower-crustal thickness of 15 km. The descending lower crust is divided into 100 km long bodies and their densities are varied independently to fit the observed Bouguer anomalies. These best models show that the major density jump occurs when the ILC reaches its maximum depth, what we interpret as the completion of the eclogitization process. The density-contrast between the crust and the mantle remains significant during the descent of the lower crust. White dots on the bottom graph of Fig. 4b represent lower-crustal microseismicity relocalized by Monsalve et al. (2006). The white solid lines on the bottom graph of Fig. 4c show the shear-wave velocity models obtained by inversion of receiver function data at individual broadband stations of the INDEPTH experiment (Kind et al., 1996), the overlying scale representing 1 km s^{-1} steps per tick in V_S. Density values that are not noted on the figures are the following: (a) ρ_6=3300, ρ_7=3250, ρ_8=3050, ρ_9=3000, and ρ_{10}=2950 kg m^{-3}. (b) ρ_6=3300, ρ_7=3100, and ρ_8=3050 kg m^{-3}. (c) ρ_6=3200, ρ_7=3100, and ρ_8=3000 kg m^{-3}.

on the P–T conditions, and ranges between 3080 and 3630 kg m^{-3}. Based on these grids and on thermo-kinematic modelling, Henry et al. (1997) proposed that the high altitude of the Himalayas is related to the absence of eclogites beneath the mountain range, due to the fast rates of underthrusting of relatively cold material. Furthermore, based on gravity data combined with numerical modelling, Cattin et al. (2001) showed that eclogitization does not take place under the High Himalayan range as expected from a steady-state local equilibrium assumption, but further North beneath the Tibetan Plateau. More recently, Tiwari et al. (2006) showed that gravity and magnetic anomalies across Sikkim can be explained with a model in which the crust beneath Tibet (between 56 and 72 km depth) is eclogitized ~100 km north of the YTS.

To explore the effect of density variation within the lower crust and to constrain its spatial extent, we first test two end-members models without and with densification, respectively, using the geometries of profile P1. Next we propose a gradual density variation that is consistent with the observed gravity anomalies for the three studied profiles.

4.1. Tests of densification of the Indian lower crust beneath Tibet

In the first test (Model 1), we suppose that Tibetan crust becomes denser with depth but we assume no density variation within the Indian lower crust (Fig. 3a). The calculated Bouguer anomaly is roughly consistent with the observed one between the Ganges plain and the High Himalaya. However in southern and central Tibet, the calculated anomaly is systematically lower than — and thus inconsistent with — the observed one. The misfit reaches up to 250 mGal in central Tibet, which

implies that the primary density contrast is located deeper than necessary (undercompensation).

In the second test (Model 2), we assume a density increase of 400 kg m^{-3} for the entire underthrust part of the ILC (beneath 35 km, Fig. 3b), thus its density contrast with the mantle is close to zero as suggested by Henry et al. (1997). However, we assume that the underthrust part remains lighter than the mantle and we do not address the question of delamination. The Bouguer anomaly corresponding to Model 2 presents a step of ~500 mGal between India and central Tibet, in agreement with the observed anomaly. Nevertheless, the calculated anomaly is systematically higher than the observed one between −200 and 500 km distance, beneath the foreland basin and the Himalayan range, with a maximum deviation of ~150 mGal, implying overcompensation in this zone.

The deviations between the calculated and observed anomalies in these two models represent end-members, and suggest a progressive density variation of the Indian lower crust. These changes occur between the foreland basin and Southern Tibet, 500 km north from the MFT, where the density of the lower crust reaches the density of the mantle. We performed similar tests on profiles P2 and P3 and obtained identical results.

4.2. Gradual density variation of the ILC along profile and lateral comparisons

To model a gradual change of the Indian lower-crustal density from 2900 to 3300 kg m^{-3}, we divide the zone between −200 and 500 km into 100 km long segments and vary their densities manually and stepwise. Numerous models have been tested to simulate northward densification, using linear density gradients on varying length as well as non-linear density changes, in order to minimize χ^2 in Eq. (2). We similarly processed all three profiles; our results (Fig. 4a–c) show many similarities but also some differences.

The similarities of the results lie in the fact that, in the very first order, the geometry of the Moho is quite similar along each profile: it starts at 35 km depth in the South and ends at about 75 km depth beneath the Tibetan plateau. The density values show that the major change in density of the Indian lower crust occurs once it reaches its maximum depth. Also, a slow gradual change from lower to higher values takes place in the descending part.

The differences between the three profiles are also linked to the geometries: the steepness and the localization of the lower crust's descent are particular to each profile. Between profile P1 and P2, the differences are small: profile P2 shows a somewhat steeper dip, located closer to the front of the range compared to profile P1, but both profiles reach their maximum depth in one ramp. This is not the case for profile P3: there is a flat part in the descent of the lower crust between two ramps, and constraints on the geometry (even if they are less tight) suggest that it plunges at a lower angle and on a longer distance than profiles P1 and P2. Thus the gradual change of density also takes place on a larger distance. One additional difference is the geometry of the foreland basin: while data are well explained by a flexural form at profiles P1 and P2, it is better represented with a shallower, flat-bottom basin at profile P3, as previously mentioned by Tiwari et al. (2006).

These results are also consistent with the detailed seismological image. The inverted receiver functions at individual stations of the INDEPTH experiment (Kind et al., 1996) show a two-step transition in shear wave velocity between the lower crust and the mantle in Southern Tibet (white lines on Fig. 4c). These receiver functions are located in a zone where the density of the Indian lower crust is constant, but lower than that of the mantle. The same features are visible at Hi-CLIMB stations in Lhasa block (Nábělek et al., 2005), and high lower-crustal velocities are observed in the northern part of the HIMNT experiment (Schulte-Pelkum et al., 2005). This two-step transition can be explained by the high density of eclogites relative to their P-wave velocity (Guéguen and Palciauskas, 1992), which leads to two impedance-contrasts: one between the bottom of Tibetan crust and the top of the eclogitized Indian lower crust, and the second between the bottom of the ILC and the top of the lithospheric mantle. (More quantitatively, following Hacker and Abers (2004), at a pressure of 20 kbar and a temperature range of 600–700 °C, we obtain a P-wave velocity of 7.5±0.1 km s^{-1} and a mantle density value of 3350±30 kg m^{-3}, the error-bars accounting for compositional variations of eclogite.)

Our findings confirm the results of Henry et al. (1997), which suggest that the extreme altitude of the Himalayas, in a zone between 100 and 200 km north of the front, can be explained by the absence of eclogites beneath them. Due to the fast subduction rate and the relatively cold temperatures, the eclogitization process is completed further North, at ~300 km from the MFT (Henry et al., 1997).

4.3. Limitations of this approach: towards a coupled petrological modelling

The ILC density at depth is estimated by taking into account large-scale observations only. This first-order

approach, neglecting the presence of local geological features, appears to be reasonable. The limited spatial extent and second-order density contrast of these features contribute to gravity anomalies only within the dispersion of the data (tens of mGals).

Also, we neglect here density variations resulting from thermal expansion and compressibility. Furthermore, the petrological relevance of the gradual density change occurring in the ILC, which is inferred from geophysical data, has not been evaluated. This evaluation requires the modelling of metamorphic transformations, in particular eclogitization at depth. This is only possible if the pressure and temperature distributions beneath Tibet are accurately established. In the next section we overcome these limitations and we combine thermo-kinematic modelling and petrogenetic grids to evaluate the petrological relevance of the density models retrieved above.

5. Integrated geophysical and petrological approach: modelling

The density of the Indian lower crust beneath the Tibetan plateau can be determined from the temperature field at depth (thermo-kinematic model) and from phase equilibria calculation (petrological modelling) for a given lower-crustal composition.

The comparison between the density distribution derived from geophysical data (see above) and that predicted by combining petrological and thermo-kinematic modelling provides an indirect way to probe the phase transformations occurring within the Indian lower crust.

5.1. Thermo-kinematic modelling

We use a finite-element thermo-kinematic model (FEAP, Finite Element Analysis Program) which solves the heat advection–diffusion equation in transient state (Zienkiewicz and Taylor, 1989) to obtain the temperature field beneath the Himalayas and Southern Tibet; including thermal expansion and compressibility. Using this modelling approach, Bollinger et al. (2006) reproduced the inverse metamorphic gradient, peak temperatures and exhumation ages, constrained by dense field observations across the Himalayan range in Central Nepal.

Our model is similar to the one presented by Bollinger et al. (2006) and is shown on Fig. 5. It includes a single thrust zone (MHT) with an accretion window, five layers of uniform physical properties within each, steady-state topography, and a convergence rate across the range of 21 mm yr^{-1}, matching the Holocene shortening rate (Lavé and Avouac, 2000). For more details, we refer to Bollinger et al. (2006) and references therein.

As our model focuses on the lower Indian crust, we update the previously used geometry according to seismological observations: the Moho beneath India is

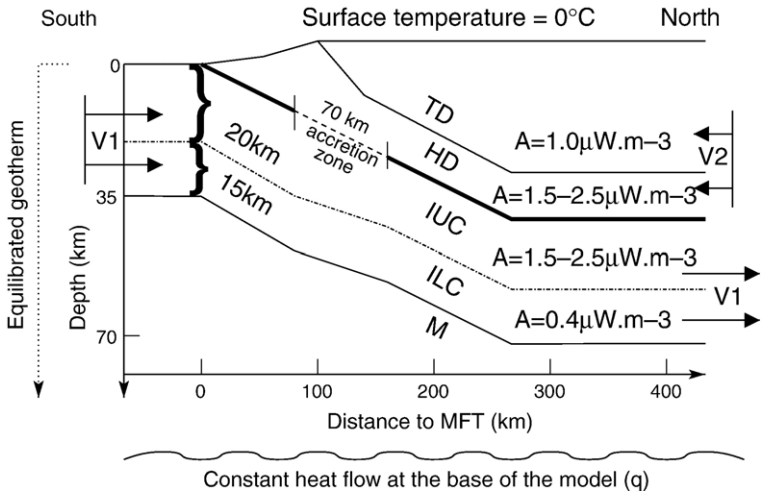

Fig. 5. Geometry, thermal parameters and boundary conditions of the thermo-kinematic model, after Bollinger et al. (2006): M: mantle; ILC: Indian Lower Crust; IUC: Indian Upper Crust; HD: Himalayan Domain; TD: Tethyan Domain. The thick solid line denotes the Main Himalayan Thrust, along which India underthrusts Tibet. The velocities of the two blocks are kept constant (underthrusting rate of V1 = 17 mm yr^{-1}, overthrusting rate of V2 = −4 mm yr^{-1}), such as the radioactive heat production of the lower crust (0.4 μW m^{-3}; Pinet et al., 1991) and of the Tethyan Domain (1.0 μW m^{-3}). The varied parameters are the basal heat flow and the radiogenic heat production in the HD and the IUC.

Table 1
Petrological model parameters, with composition of the lower crust in weight percent (Rudnick and Fountain, 1995; Rudnick and Gao, 2003)

Model name	MW (wet)	MD (dry)	MPH (1% water)
SiO_2	53.961	53.961	53.422
Al_2O_3	17.078	17.078	16.907
FeO_x	8.660	8.660	8.573
MgO	7.316	7.316	7.243
CaO	9.691	9.691	9.594
Na_2O	2.678	2.678	2.651
K_2O	0.616	0.616	0.610
H_2O	0.0–5.54 [a]	0.0	1.0
Total	100.00	100.00	100.00
Hydration	Full	None	Partial

[a] For the MW model, the H_2O component is in excess (i.e. fully hydrated assumption). This corresponds to a hydration level for the ILC (amount of water contained in hydrous minerals) comprised between 0.24 wt.% and 5.11 wt.% H_2O depending on the P–T conditions along the P–T path derived here. The hydration level of the ILC before it is underthrust amounts to ca. 3 wt.% H_2O.

located at 35 km, the lower crust has a constant thickness of 15 km, and the descent of the plate is continued until the Moho reaches a depth of 73 km.

Following previous studies (Henry et al., 1997; Bollinger et al., 2006), we test the effect of two thermal parameters: upper crustal radiogenic heat production A, and basal heat flow of the model q. The latter parameter is varied between 15 mW m^{-2} (Pinet et al., 1991; Gupta, 1993) and 30 mW m^{-2} (Rao et al., 1976) by steps of 2.5 mW m^{-2}. Since the radiogenic heat production of the Indian upper crust beneath the Himalayas, of the Lesser Himalayas and of the overlying High Himalayan Crystalline are still largely unconstrained, locally ranging between 0.7 and 5 μW m^{-3} (Menon et al., 2003), we have considered that 1.5 and 2.5 μW m^{-3} represent mean low and high values in these regions and adopted these end-members for A. These values appear to be consistent with the few heterogeneous local estimates of the High Himalayan crystalline radiogenic heat production (England et al., 1992). Aside from the above parameters, the model follows the one in Bollinger et al. (2006) including the granodioritic composition of the Himalayan and Tethyan domain, as well as of the Indian upper crust. The composition of the Indian lower crust is discussed in the following section.

5.2. Petrological modelling

To assess the gravity anomalies produced by a density-distribution based on a thermo-kinematic model, one needs to know the dependence of density as a function of temperature and pressure.

We calculated mineral compositions and modes for an average lower crust composition as a function of pressure and temperature using Perple_X (Connolly, 2005). For a given composition and a set of solution phases, Gibbs energy is minimized to map the phase relations on that composition. Then, physical properties, such as density, are derived. A high density resolution (in the P–T space) and a high accuracy level can be achieved with this software since mineral compositional variations with P and T are taken into account along with thermal expansion and compressibility for individual phases. In all cases, density models derived from Perple_X assume thermo-chemical equilibrium at all scales.

We use an average lower-crustal composition based on Rudnick and Fountain (1995) and Rudnick and Gao (2003) with eight major oxide components (including water; see Table 1). The selected solid-solution data and the corresponding thermodynamic sources are listed in Table 2. Actually, we have considered three different lower crust compositions differing only in their water content:

Table 2
Selected solid solutions for petrological modelling, corresponding formulae and thermodynamic references

Phase	Formula	Source
Biotite	$K[Mg_xFe_yMn_{1-x-y}]_{3-w}Al_{1+2w}Si_{3-w}O_{10}(OH)_2, x+y\le 1$	Powell and Holland (1999)
Orthopyroxene	$[Mg_xFe_{1-x}]_{2-y}Al_{2y}Si_{2-y}O_6$	Holland and Powell (1996)
Clinopyroxene	$Na_{1-y}Ca_yMg_{xy}Fe_{(1-x)y}Al_{1-y}Si_2O_6$	Holland and Powell (1996)
Muscovite	$K_xNa_{1-x}Mg_yFe_zAl_{3-2(y+z)}Si_{3+y+z}O_{10}(OH)_2$	Holland and Powell (1998)
Clinoamphibole	$Ca_{2-2w}Na_{z+2w}[Mg_xFe_{1-x}]_{3+2y+z}Al_{3-3y-w}Si_{7+w+y}O_{22}(OH)_2, w+y+z\le 1$	Wei and Powell (2003); White et al. (2003)
Garnet	$Fe_{3x}Ca_{3y}Mg_{3z}Mn_{3(1-x-y-z)}Al_2Si_3O_{12}, x+y+z\le 1$	Holland and Powell (1998)
Feldspar	$K_yNa_xCa_{1-x-y}Al_{2-x-y}Si_{2+x+y}O_8, x+y\le 1$	Fuhrman and Lindsley (1988)
Talc	$[Mg_xFe_{1-x}]_{3-y}Al_{2y}Si_{4-y}O_{10}(OH)_2$	
Sapphirine	$[Mg_xFe_{1-x}]_{4-y/2}Al_{9-y}Si_{2-y/2}O_{20}$	Holland and Powell (1998)
Spinel	$Mg_xFe_{1-x}Al_2O_4$	
Chlorite	$[Mg_xFe_wMn_{1-x-w}]_{5-y+z}Al_{2(1+y-z)}Si_{3-y+z}O_{10}(OH)_8, x+w\le 1$	Holland et al. (1998)
Chloritoid	$Mg_xFe_yMn_{1-x-y}Al_2SiO_5(OH)_2, x+y\le 1$	White et al. (2000)

The thermodynamic data used by the Perple_X code are based on Holland and Powell (1998, updated in 2002). The compositional variables w, x, y, and z may vary between zero and unity and are determined in Perple_X as a function of computational variables by free-energy minimization.

– MW (Mafic and Wet) is a fully hydrated lower crust. Full hydration means that the water content in MW corresponds to the minimum water content required to stabilize all the hydrous phases (and in the same proportion) as in a water-saturated system under greenschist/blueschist facies conditions, *i.e.* conditions at which the Indian lower crust enters the Himalayan subduction. This hydration level is derived from the Perple_X output (5.54 wt.%).
– MD (Mafic and Dry) is a completely dry lower crust without any hydrated mineral. We suppose here that the Indian Lower Crust experienced granulitic P–T conditions without being rehydrated before entering the Himalayan subduction.
– MPH (Mafic and Partially Hydrated) is a partially hydrated lower crust (1 wt.% H_2O). This simulates a scenario where the Indian Lower Crust first experienced amphibolitic conditions (with no subsequent hydration event) and then re-equilibrated under greenschist/blueschist conditions prior to underthrusting.

6. Results and discussion: constraints on eclogitization kinetics of the Indian lower crust

For the sake of simplicity, the following sections are structured in a way that the parameters of the ILC density model based on thermo-kinematic and petrologic constraints which fits better the geophysical data, called "best fit model" hereinafter, are presented first. Then the sensitivity of these parameters is discussed in detail, and the various constraints on the thermo-kinematic and petrologic modelling are addressed. Finally, we show how this combined approach can provide new constraints on the eclogitization kinetics of the ILC.

6.1. The best fit model

Fig. 6 shows the best fit model solution of this study. It yields gravity anomalies in very good agreement with measurements, leading to a misfit lower than 50 mGal, and in many cases lower than 25 mGal, which corresponds to the estimated error of our dataset. This result clearly confirms the major role of eclogitization in the support of Tibet. The density distribution of this model is obtained by using a temperature field calculated with $A=2.5$ μW m^{-3} and $q=15$ mW m^{-2}, an amphibolitic crust (MPH model) and a delay in eclogitization, which prescribes that eclogitization occurs between 300 and 350 km north of the MFT rather than between 0 and 80 km. Constraints on the above three conditions, together with the path of the Indian lower crust in the P–T space, are described in the following sections.

6.2. Petrological constraints on the temperature field

The two criteria used to assess the temperature field of the models are the temperature at the Moho (at 35 km depth) beneath the Indian shield, T_{MI}, and the temperature of the eclogitized Indian lower crust beneath Tibet, T_{ET}. The obtained values in all tested models for both T_{MI} and T_{ET} are shown on Fig. 7 and are discussed below.

The temperature at the Moho varies between 392 and 583 °C for the "cold" ($A=1.5$ μW m^{-3}), and between 472 and 660 °C for the "hot" ($A=2.5$ μW m^{-3}) thermo-kinematic models. This is equivalent to a step of about +12.5 °C for an increase of basal heat flow of 1 mW m^{-2} at constant A, and to an average difference of 78 °C between "hot" and "cold" models of equal basal heat flow. Our best fit model uses the same thermal parameters as Bollinger et al. (2006), and shows a T_{MI} of 472 °C. This is consistent with previous work by Henry et al. (1997), which favours models with T_{MI} between 417 and 463 °C, and rejects models with T_{MI} of 684 °C, based on heat flow measurements in the Indian shield. Putting the acceptable range of T_{MI} to around 425–525 °C (shaded region in Fig. 7a), the basal heat flow is 15±4 mW m^{-2} for the "hot", and 21±4 mW m^{-2} for the "cold" models, or any equivalent combination in between.

The temperature reached by the underthrust Indian lower crust beneath Tibet provides another constraint. T_{ET} (at 350 km) varies between 565 and 753 °C for the "cold", and 700 and 888 °C for the "hot" models. The temperature increase is the same for $\Delta q=+1$ mW m^{-2} as above, but the average difference between "hot" and "cold" models at equal basal heat flow is increased to 135 °C. Examples from Holsnøy Island in the Bergen Arcs complex show that the solidus is ~700 °C at 16–19 kbar for wet eclogites (Andersen et al., 1991). Experimental studies reveal similar values: the solidus of wet mafic rocks at 20 kbar is around 700 °C, and a 1% water-content rock produces about 10% melt at this temperature (Rushmer, 1991). More recently, Raimbourg et al. (2007) measured an average of 718 °C and 20.5 kbar on samples from Holsnøy Island, without observing any sign of melting. As our model is not fully hydrated, we can expect a solidus slightly above these values (dashed line in Fig. 7b). Comparing the obtained values of T_{ET} with the above estimation of the solidus, we eliminate the "hot" models above $q=17$ mW m^{-2}, the "cold" models above 28 mW m^{-2}, or any equivalent combination in between.

In summary, the best fit model with $A=2.5$ μW m^{-3} and $q=15$ mW m^{-2} is close to the highest allowed temperature without melting. This model does not change the upper crustal thermal structure of Bollinger et al. (2006). It therefore still satisfies both the thermochronological

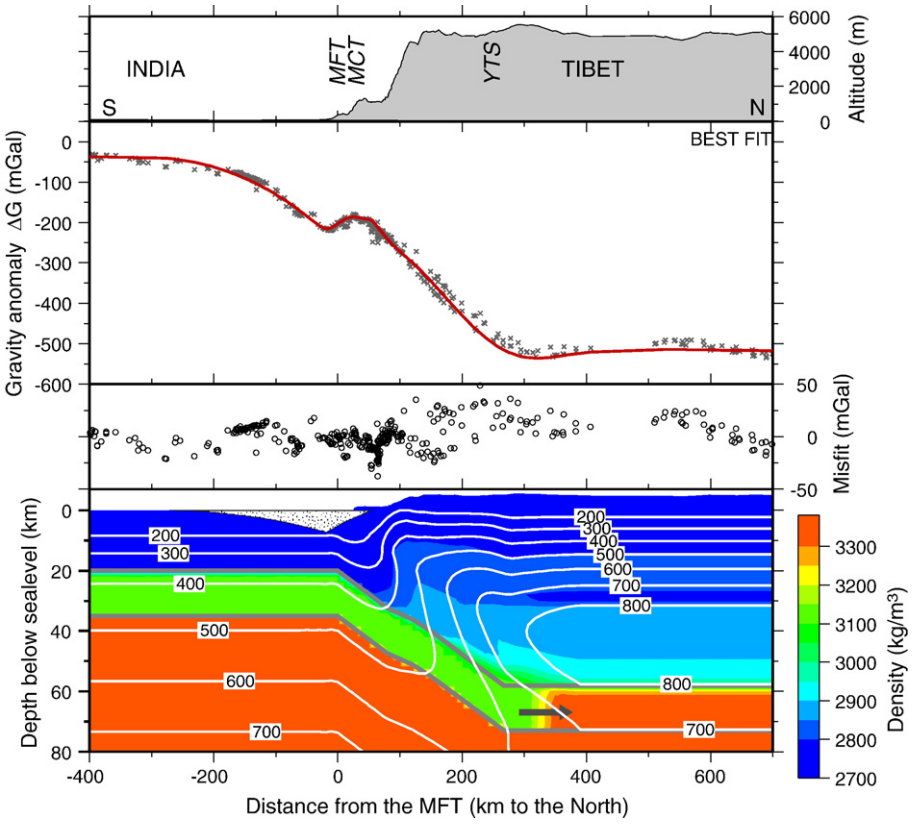

Fig. 6. The best fit density-model (graphs as on Fig. 3), based on: i) the thermal field from thermo-kinematic modelling (white contours and value in °C, $A=2.5\ \mu W\ m^{-3}$ and $q=15\ mW\ m^{-2}$); ii) petrogenetic grids corresponding to a mafic lower crust with 1 wt.% water content (Fig. 7); iii) a delay of eclogitization until 300 km. The arrow marks the path of the Indian lower crust and the place where transformation into eclogite takes place. See Fig. 7 and Section 6 for more details. The densities of the upper crust and the mantle are based on the petrogenetical grids of Bousquet et al. (1997).

and peak temperature dataset available through the underplated Lesser Himalayas and its overlying crystalline nappes constraining the paleo-location of the 350 °C to 550 °C isotherm under the Himalayas. An uncertainty at ±50 °C is estimated on these mid-crustal isotherms, deduced from the uncertainty on the thermometrical

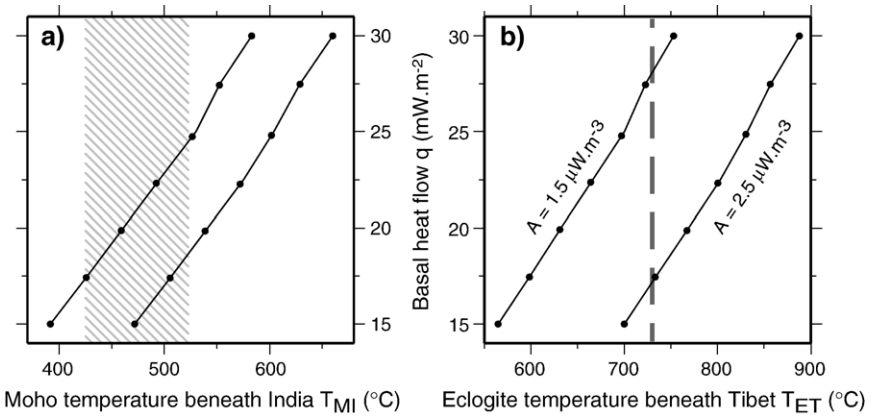

Fig. 7. Temperature at the Moho beneath the Indian shield (T_{MI}) and within the eclogitized Indian lower crust beneath Tibet (T_{ET}), as a function of basal heat flow (q) and radiogenic heat production of the upper crust (A). In (a), the shaded region is the acceptable range of T_{MI}. In (b) the dashed line is approximate melting temperature of lowly hydrated mafic rocks.

(Beyssac et al., 2004) and thermochronological dataset as well as on the closure temperature for Ar in muscovite and hornblende (*e.g.* McDougall and Harrison, 1999). In the meantime, other models with lower radiogenic heat production and higher basal heat flow (until $A=1.5$ μW m^{-3} and $q=21$ mW m^{-2}, "cold") are equivalent and possible. In term of synthetic gravity anomalies, this set of solution reproduces very well the observed difference between values in India and Tibet (~500 mGal); as of the sensitivity of the solution, an increase of 4 mW m^{-2} in a "cold" model heat flow would lower this difference by ~30 mGal.

6.3. The choice of the petrological model

The most sensitive parameters that differentiate the three petrological models (MW, MD and MPH) are the horizontal localization of density increase, and the temperature of this zone. Based on gravity modelling in Section 4.2, the highest amplitude change in the density of the lower crust is located at around 300 km north of the MFT. On the other hand, the path of the Indian lower crust in temperature–pressure space (Fig. 8) shows that the major increase of density is expected to occur at the transition to the blueschist facies, close to the front (between 0 and 100 km horizontal distance), irrespective of the level of hydration (dry, partially hydrated, or wet) of the ILC. The temperature of the ILC at around 300 km is 150±50 °C higher than the temperature of the zone where the density change is expected to occur from P–T–ρ grids, and this is true for all thermal models. Such transformation delay clearly shows that the kinetics of the eclogitization process should be considered for the ILC, since it influences considerably its density distribution, and thus the gravity anomaly.

Reaction overstepping by 150±50 °C is unlikely in water-saturated systems since these could not survive for geological timescales (Wood and Walther, 1983). A completely dry system is also unlikely: examples from the Bergen Arc in Norway show that a dry crust subducted into roots of continental collision zones undergoes eclogitization only if hydrous fluids are available, independently of the crossing of equilibrium boundaries (Austrheim et al., 1997). Similar triggering of eclogitization in subduction zones is also known, for example in Zambia (John and Schenk, 2003). In this context, fluid is thought to infiltrate from the hydrated mantle wedge; however, in our case of underthrusting, there is no similar argument for localized fluid infiltration. These considerations lead us to favour petrological model MPH (1 wt.%

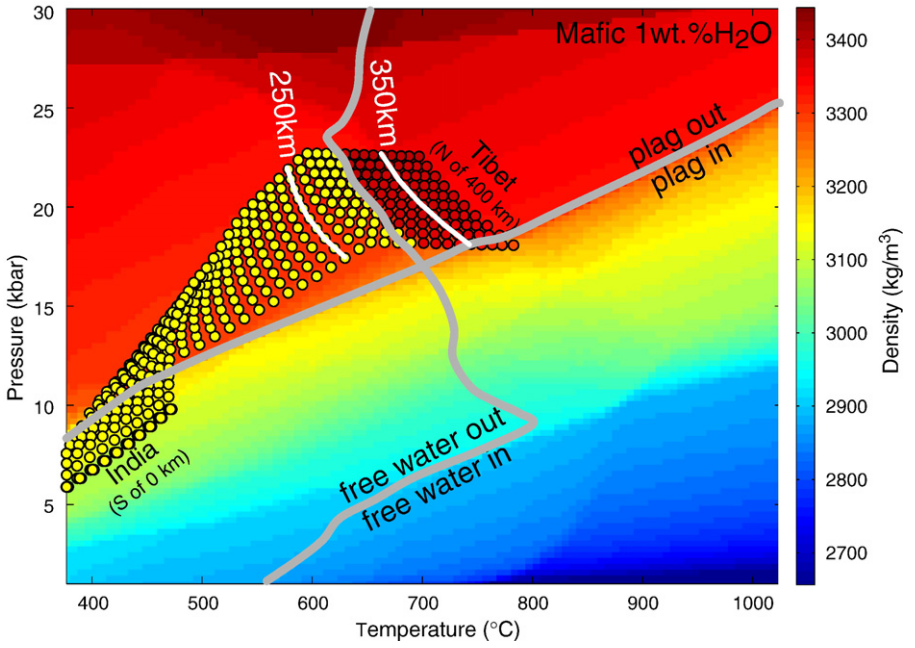

Fig. 8. Density grid for a mafic composition with 1 wt.% water content. Grey lines show the stability limit of plagioclase and of free water in the system. The black contoured circles show the P–T distribution for the best fit model (Fig. 6) within the Indian Lower Crust during its underthrusting from South to North. The white lines delineate the position of the ILC at 250 and 350 km north of the MFT. As the disappearance of plagioclase, mainly through the breakdown of albite into jadeite+quartz, does not release water, it can be delayed (overstepped), and the ILC can keep its initial density until it crosses the dehydration line and eclogitizes rapidly. This is also represented by the colours filling the black circles, showing the actual density of the ILC (including the delay). See Section 6.4 for more details.

H_2O) as the most realistic solution, a model for which free water is however not available along the whole ILC underthrusting path. This is in line with Henry et al. (1997), who discuss that, in the case of the Precambrian Indian crust, whereas the water necessary to form all hydrated minerals in the blueschist facies (~5% in the MW model) may not be available, a water content of about 1% can probably be found.

The gravity anomalies associated to a mafic lower crust with three different hydration levels (MW, MD and MPH) are shown on Fig. 9a. The primary point here is to reproduce the observed absolute step between the two endpoints of the profile. The synthetic anomalies corresponding to the three models actually support the petrological considerations developed above. A mafic lower crust hydrated at 1 wt.% H_2O (MPH) reproduces well the difference of ~500 mGal between India and Tibet, whereas synthetic anomalies obtained by considering either the wet or the dry model are clearly off, situated about 80 mGal above and 60 mGal below the data, respectively. However, between ~50 and ~350 km horizontal distance, the synthetic anomalies of the MPH model follow the same gradient as the observations, but are offset by +100 mGal. This is due to the fact that the locus of density-change in the ILC is calculated assuming thermo-chemical equilibrium (*i.e.* no reaction overstepping).

6.4. Implications for the eclogitization kinetics

Fig. 9b shows three different reaction kinetics for the eclogitization of the ILC (inset), and the corresponding gravity anomalies. The curve assuming thermochemical equilibrium, where the change in density occurs fully and exactly where it is anticipated by the MPH petrogenetic grid, is reported from Fig. 9a. The low-kinetics case is based on the assumption that the eclogitization process is sluggish: it begins as it is expected from the petrogenetic grid, but the transformation progresses linearly with distance (thus time) until its completion at 300 km horizontal distance. We see that the synthetic gravity anomalies still fail to follow the observed data. Finally, the best fit model (see also Fig. 6) is where the eclogitization process is delayed (overstepped) until 300 km and then occurs within 50 km. The synthetic anomaly fits very well to the observed one, included the gravity-low at ~300 km. It should be noted that other types of density evolutions can also fit the observations, provided that the transition proceeds in the 250–350 km interval and that it is monotonous. We also note that density variations due to compressibility and thermal expansion partially cancel out in the descending part of the ILC, thus the remaining effect, being less than 10% of the density change related to eclogitization, is neglected.

Fig. 8 summarizes the non-gravimetric constraints of our models. It shows the petrogenetic grid of the MPH model, with two lines enhanced in grey: the limit of stability of plagioclase and of free water in the system (dehydration line), respectively. The circles show the path of the underthrusting Indian lower crust in the P–T field with the colours corresponding to its density. We claim that, along this path, the conversion of the plagioclase component into garnet and/or clinopyroxene,

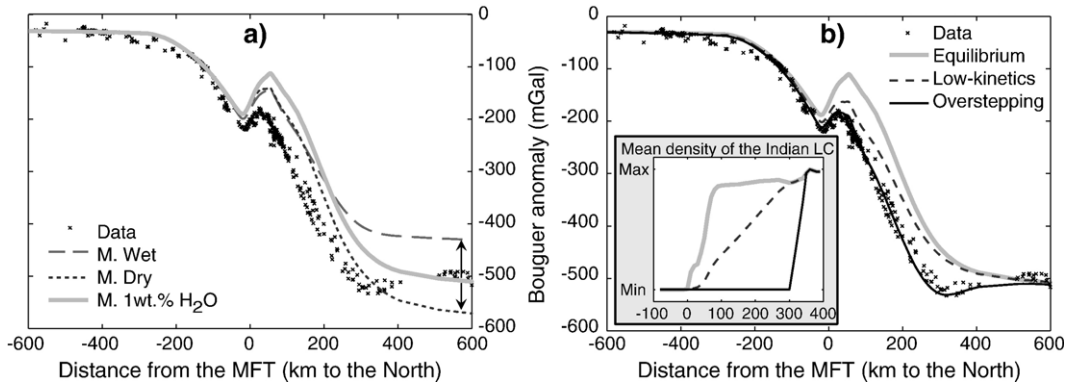

Fig. 9. (a) The effect of the choice of hydration level on gravity anomalies (with thermal parameters of $A=2.5\ \mu W\ m^{-3}$ and $q=15\ mW\ m^{-2}$). The first step in resolving the problem is to reproduce the step of ~500 mGal in Bouguer anomalies between the two endpoints of the profile. While the 1 wt.% water-content model reproduces the observed step between India and Tibet, the wet model falls short of it, and the dry model step is too large, as it is emphasized by the arrows at ~600 km. (b) The effect of reaction kinetics on gravity anomalies, using the 1 wt.% water-content model. For the equilibrium and slowed-down (see inset) models of eclogitization, the calculated anomalies are clearly different from observations between 0 and 400 km. The best fit model is where the eclogitization is delayed to about 300 km (see inset, as well as Figs. 6 and 8).

which does not release water, is kinetically hindered. The density change predicted by the petrogenetic grid (equilibrium conditions) does not actually occur. Later on, when the P–T conditions of this metastable lower crust reach the dehydration line, free water is produced which catalyses the metamorphic reactions (water is provided under these conditions by amphibole and epidote breakdown). Eclogitization occurs then relatively quickly due to the large temperature overstep (150±50 °C), and density reaches its maximum value (equilibrium assemblage).

We highlighted the position of the Indian lower crust at 250 and 350 km, which encompass the dehydration line in this pressure range (Fig. 8). On the one hand, they are the limits of the zone until which eclogitization is delayed, and also inside which we cannot distinguish between different densification models on the basis of gravity. On the other hand, this ±50 km zone corresponds to an uncertainty of ±50 °C in temperature, which is similar to the temperature constraints obtained when assessing the thermal field (the ±4 mW m^2 corresponding to ±50 °C). Thus, even if a smaller trade-off is possible between eclogitization localization and the thermal structure, it is realistic to consider the two white lines as a lower and upper bound to the temperature field, and to assume that the key factor in the eclogitization process is the release of free water in the system.

We consider that the geometry used in the thermo-kinematic model is within the error-bars of profile P2, and the obtained results are roughly valid for this profile. The main difference in the geometry of profile P2 compared to profile P1 is a steeper descent of the lower crust to its maximal depth (Fig. 4b). On the same figure, we reported the relocated microseismicity data of Monsalve et al. (2006). A clear cluster of events is visible between 140 and 200 km North of the MFT and at a depth of ~60–80 km. This zone of microseismicity is located where the ILC reaches its maximum depth, *i.e.* where eclogitization is catalyzed due to water release by dehydration reactions. The observed microseismicity is therefore an additional argument for the release of free water in the eclogitization zone of the ILC; the liberated water increases pore pressure and causes failure at previously stable stress conditions.

Concerning profile P3, we have followed the same modelling steps with a more accurate geometry. The calculations are less well constrained as gravity anomaly data show more dispersion in the region of interest (between 100 and 400 km), but our results show that a delay of ~200 km is probable, followed by a transition zone of kinetics that is longer than in the best fit model.

7. Conclusions

This study brings new constraints on metamorphic reaction overstepping and kinetics at field scale from petrological models, gravity anomalies and seismological data at the southern border of the Tibetan Plateau.

We compile both seismological and Bouguer anomaly data along three arc-perpendicular profiles. Forward gravity modelling based on the observed geometries and varied densities show that Airy-type isostatic compensation is unlikely to occur, as it yields unrealistic densities. This suggests that higher density eclogites are required to support the Tibetan Plateau. Multilayer models show that Indian lower crust eclogitization is completed once the ILC reaches its maximal depth.

In order to interpret these geophysical data in a petrological frame:

(i) we performed thermo-kinematic modelling to obtain the temperature field in the area;
(ii) we calculated realistic petrogenetic (pressure–temperature–density) grids;
(iii) we tested wet, dry, and partially hydrated mafic lower-crustal composition models.

This led us to probe different types of reaction kinetics for the eclogitization of the ILC.

The Indian lower crust follows a blueschist–eclogite path in the temperature–pressure space. The derived density profiles were used for forward modelling of Bouguer anomalies. Comparison of the different models shows that at least a small amount of water should be contained in the ILC prior to underthrusting, and that the plagioclase-consuming reactions (no water release) are overstepped, and therefore densification is delayed. This delay lasts until the attainment of the dehydration reactions where eclogitization will occur in less than 100 km horizontal distance. Considering the underthrusting rate (17 mm yr^{-1}), the eclogitization occurs quickly (less than 6 My). Even when considering the uncertainties of the localization of eclogitization and of the temperature field, the appearance of free water in the system remains the key factor in the eclogitization process. The partial eclogitization of mafic compositions (gabbroic rocks from Zambia) along a blueschist–eclogite path has already been documented by John and Schenk (2003). They also reach the conclusions that large overstepping of reaction boundaries has occurred and that the gabbro-eclogite transformation was triggered by the presence of a free fluid-phase.

The derivation of mineral reaction kinetics is one of the challenges of metamorphic petrology. Even though reaction progress can be evaluated, reaction duration is difficult to assess from field-based observations. All attempts that have been made to derive reaction rates in metamorphic systems (*e.g.* Baxter and DePaolo, 2000; Carlson et al., 1995; Vance and O'Nions, 1992; Christensen et al., 1989) show that reaction kinetics in nature are lower, by several orders of magnitude, than those obtained experimentally (see Baxter, 2003 for a review). Baxter (2003) suggests that water availability during metamorphism can account for this discrepancy. For example, Rubie (1986) has proposed that at deep crustal levels, fluid-present conditions could be transitory and related to relatively short dehydration events. This is in line with the interpretation of our gravity dataset in the frame of phase equilibria which strongly suggests that the water released by mineral dehydration can trigger eclogitization reactions. This result emphasizes how the sluggishness of nucleation kinetics can be a source of disequilibrium during metamorphism as already pointed out by Rubie (1998). Our new type of time-resolved constraint on the eclogitization process, which suggests that crystallization (nucleation and growth) of the stable mineral assemblage can be delayed by at least 100 °C under free-fluid absent conditions, clearly prompts the investigation of the role of water on mineral nucleation kinetics.

Acknowledgements

The authors would like to thank all parties that have helped to complete the geophysical datasets in this study. Many thanks to Gaspar Monsalve for providing the HIMNT microseismicity data. The paper greatly benefited from discussions with Christian Chopin on petrology, metamorphic facies and reaction kinetics; with Julia de Sigoyer on petrology and crustal composition; and with Marie-Pierre Doin on modelling. We acknowledge Christian Chopin for the thorough review of the manuscript, two anonymous reviewers for their comments that have helped to clarify our modelling choices, as well as the Editor Claude Jaupart for his suggestions and help. Petrogenetic calculations were performed using the Perple_X code (www.perplex.ethz.ch; Connolly, 2005). Finite-element computations were performed using the FEAP program, developed by R. Taylor at the University of California at Berkeley (http://www.ce.berkeley.edu/rlt/feap/). Figs. 1, 3, 4, 6 and 7 were prepared by the GMT software package (Wessel and Smith, 1991). We thank the French DYETI programme for support. Project Hi-CLIMB is supported by the U.S. NSF Continental Dynamics Program, EAR 9909609.

References

Airy, G.B., 1855. On the computation of the effect of the attraction of mountain-masses, as disturbing the apparent astronomical latitude of stations in geodetic surveys. Phil. Trans. Roy. Soc. Lond. 145, 101–104.

Andersen, T., Austrheim, H., Burke, E.A.J., 1991. Mineral fluid melt interactions in high-pressure shear zones in the Bergen Arcs nappe complex, Caledonides of Norway — implications for the fluid regime in Caledonian eclogite-facies metamorphism. Lithos 27 (3), 187–204.

Austrheim, H., Erambert, M., Engvik, A.K., 1997. Processing of crust in the root of the Caledonidan continental collision zone: the role of eclogitization. Tectonophysics 273, 129–153.

Avouac, J.-P., 2003. Mountain building, erosion, and the seismic cycle in the Nepal Himalaya. Adv. Geophys. 46, 1–80. doi:10.1016/S0065-2687(03)46001-9.

Barazangi, M., Ni, J., 1982. Velocities and propagation characteristics of Pn and Sn beneath the Himalayan arc and Tibetan Plateau: possible evidence for underthrusting of Indian continental lithosphere beneath Tibet. Geology 10, 179–185.

Baxter, E.F., 2003. Natural constraints on metamorphic reactions rates. In: Vance, D., Müller, W., Villa, I.M. (Eds.), Geochronology, Linking the Isotopic Record with Petrology and Textures. Geol. Soc., London, Spec. Publ., vol. 220, pp. 183–202.

Baxter, E.F., DePaolo, D.J., 2000. Field measurement of slow metamorphic reaction rates at temperatures of 500° to 600 °C. Science 288, 1411–1414.

Bettinelli, P., Avouac, J.-P., Flouzat, M., Jouanne, F., Bollinger, L., Willis, P., Chitrakar, G.R., 2006. Plate motion of India and interseismic strain in the Nepal Himalaya from GPS and Doris measurements. J. Geod. 80, 567–589.

Beyssac, O., Bollinger, L., Avouac, J.-P., Goffé, B., 2004. Thermal metamorphism in the Lesser Himalaya of Nepal determined from Raman spectroscopy of carbonaceous material. Earth Planet. Sci. Lett. 225, 233–241.

Bollinger, L., Avouac, J.-P., Beyssac, O., Catlos, E.J., Harrison, T.M., Grove, M., Goffé, B., Sapkota, S., 2004. Thermal structure and exhumation history of the Lesser Himalaya in central Nepal. Tectonics 23, TC5015. doi:10.1029/2003TC001564.

Bollinger, L., Henry, P., Avouac, J.-P., 2006. Mountain building in the Nepal Himalaya: thermal and kinematic model. Earth Planet. Sci. Lett. 244, 58–71.

Bousquet, R., Goffé, B., Henry, P., Le Pichon, X., Chopin, C., 1997. Kinematic, thermal and petrological model of the Central Alps: lepontine metamorphism in the upper crust and eclogitisation of the lower crust. Tectonophysics 273, 105–127.

Carlson, W.D., Denison, C., Ketcham, R.A., 1995. Controls on the nucleation and growth of porphyroblasts: kinetics from natural textures and numerical models. Geol. J. 30, 207–225.

Cattin, R., Avouac, J.-P., 2000. Modeling mountain building and the seismic cycle in the Himalaya of Nepal. J. Geophys. Res. 105, 13389–13407.

Cattin, R., Martelet, G., Henry, P., Avouac, J.-P., Diament, M., Shakya, T.R., 2001. Gravity anomalies, crustal structure and thermomechanical support of the Himalaya of Central Nepal. Geophys. J. Int. 147, 381–392.

Christensen, N., Mooney, W., 1995. Seismic velocity structure and composition of the continental crust; a global view. J. Geophys Res. 100, 9761–9788.

Christensen, J.N., Rosenfeld, J.L., DePaolo, D.J., 1989. Rates of tectonometamorphic processes from rubidium and strontium isotopes in garnet. Science 244, 1465–1469.

Connolly, J.A.D., 2005. Computation of phase equilibria by linear programming: a tool for geodynamic modeling and its application to subduction zone decarbonation. Earth Planet. Sci. Lett. 236, 524–541.

England, P., Le Fort, P., Molnar, P., Pêcher, A., 1992. Heat sources or Tertiary metamorphism and anatexis in the Annapurna-Manaslu region (Central Nepal). J. Geophys. Res. 97, 2107–2128.

Fuhrman, M.L., Lindsley, D.H., 1988. Ternary-feldspar modeling and thermometry. Am. Mineral. 73, 201–215.

Guéguen, Y., Palciauskas, V., 1992. Introduction à la physique des roches. In: Hermann (Ed.), des sciences et des arts, Paris. 299 pp.

Gupta, M.L., 1993. Is the Indian shield hotter than other Gondwana shields? Earth planet. Sci. Lett. 115, 275–285.

Hacker, B.R., Abers, G.A., 2004. Subduction factory 3: an excel worksheet and a macro for calculating the densities, seismic wave speeds, and H_2O content of minerals and rocks at pressure and temperature. Geochem. Geophys. Geosys. 5 (1), Q01005. doi:10.1029/2003GC000614.

Hauck, M.L., Nelson, K.D., Brown, L.D., Zhao, W., Ross, A.R., 1998. Crustal structure of the Himalayan orogen at ~90° east longitude from Project INDETPH deep reflection profiles. Tectonics 17 (4), 481–500.

Henry, P., Le Pichon, X., Goffé, B., 1997. Kinematic, thermal and petrological model of the Himalayas: constraints related to metamorphism within the underthrust Indian crust. Tectonophysics 273, 31–56.

Hetényi, G., Cattin, R., Vergne, J., Nábělek, J.L., 2006. The effective elastic thickness of the India Plate from receiver function imaging, gravity anomalies and thermomechanical modelling. Geophys. J. Int. 167, 1106–1118.

Holland, T., Powell, R., 1996. Thermodynamics of order-disorder in minerals. 2. Symmetric formalism applied to solid solutions. Am. Mineral. 81, 1425–1437.

Holland, T.J.B., Powell, R., 1998. An internally consistent thermodynamic data set for phases of petrological interest. J. Metamorph. Geol. 16, 309–343.

Holland, T., Baker, J., Powell, R., 1998. Mixing properties and activity-composition relationships of chlorites in the system MgO–FeO–Al_2O_3–SiO_2–H_2O. Eur. J. Mineral. 10, 395–406.

Jackson, M., Bilham, R., 1994. Constraints on Himalaya deformation inferred from vertical velocity fields in Nepal and Tibet. J. Geophys. Res. 99, 13897–13912.

Jin, Y., McNutt, M.K., Zhu, Y.S., 1996. Mapping the descent of the Indian and Eurasian plates beneath the Tibetan Plateau from gravity anomalies. J. Geophys. Res. 101, 11275–11290.

John, T., Schenk, V., 2003. Partial eclogitisation of gabbroic rocks in a late Precambrian subduction zone (Zambia): prograde metamorphism triggered by fluid infiltration. Contrib. Mineral. Petrol. 146, 174–191.

Jull, M., Kelemen, P.B., 2001. On the conditions for lower crustal convective instability. J. Geophys. Res. 106, 6423–6446.

Kind, R., Ni, J., Zhao, W., Wu, J., Yuan, X., Zhao, L., Sandvol, E., Reese, C., Nabelek, J., Hearn, T., 1996. Evidence from earthquake data for a partially molten crustal layer in Southern Tibet. Science 274, 1692–1694.

Kind, R., Yuan, X., Saul, J., Nelson, D., Sobolev, S.V., Mechie, J., Zhao, W., Kosarev, G., Ni, J., Achauer, U., Jiang, M., 2002. Seismic images of crust and upper mantle beneath Tibet: evidence for Eurasian plate subduction. Science 298, 1219–1221.

Lavé, J., Avouac, J.-P., 2000. Active folding of fluvial terraces across the Siwaliks Hills. J. Geophys. Res. 105, 5735–5770.

Le Fort, P., 1986. Metamorphism and magmatism during the Himalayan collision. Collision TectonicsGeol. Soc. Spec. Publ., vol. 19, pp. 159–172.

Le Pichon, X., Henry, P., Goffé, B., 1997. Uplift of Tibet: from eclogites to granulites. Tectonophysics 273, 57–76.

Ligorría, J., Ammon, C.J., 1999. Iterative deconvolution and receiver-function estimation. Bull. Seism. Soc. Am. 89 (5), 1395–1400.

Lyon-Caen, H., Molnar, P., 1983. Constraints on the structure of the Himalaya from an analysis of gravity anomalies and a flexural model of the lithosphere. J. Geophys. Res. 88 (B10), 8171–8191.

Martelet, G., Sailhac, P., Moreau, F., Diament, M., 2001. Characterization of geological boundaries using 1-D wavelet transform on gravity data: theory and application to the Himalayas. Geophysics 66 (4), 1116–1129.

McDougall, I., Harrison, T.M., 1999. Geochronology and Thermochronology by the 40Ar/39Ar Method. Oxford Univ. Press, New York. 269 pp.

Menon, R., Kumar, P.S., Reddy, G.K., Srinivasan, R., 2003. Radiogenic heat production of Late Archaean Bundelkhand granite and some Proterozoic gneisses and granitoids of central India. Curr. Sci. 85, 634–638.

Monsalve, G., Sheehan, A., Schulte-Pelkum, V., Rajaure, S., Pandey, M.R., Wu, F., 2006. Seismicity and one-dimensional velocity-structure of the Himalayan collision zone: earthquakes in the crust an upper mantle. J. Geophys. Res. 111, B10301. doi:10.1029/2005JB004062.

Nábělek, J.L., Vergne, J., Hetényi, G., 2005. Project Hi-CLIMB: a synoptic view of the Himalayan collision zone and Southern Tibet. EoS Trans. AGU 86 (52) Fall Meet. Suppl., Abstract T52A-02.

Nelson, K.D., et al., 1996. Partially molten middle crust beneath Southern Tibet: synthesis of project INDEPTH results. Science 274, 1684–1688.

Ni, J., Barazangi, M., 1983. High-frequency seismic wave propagation beneath the Indian Shield, Himalayan Arc, Tibetan Plateau and surrounding regions: high uppermost mantle velocities and efficient S_n propagation beneath Tibet. Geophys. J. R. Astron. Soc. 72, 665–689.

Owens, T.J., Zandt, G., 1997. Implications of crustal property variations for models of Tibetan plateau evolution. Nature 387, 37–43.

Patriat, P., Achache, J., 1984. India–Eurasia collision chronology has implications for shortening and driving mechanism of plates. Nature 311, 615–621.

Pinet, C., Jaupart, C., Mareschal, J.-C., Gariepy, C., Bienfait, G., Lapointe, R., 1991. Heat flow and structure of the lithosphere in the eastern Canadian shield. J. Geophys. Res. 96, 19941–19963.

Powell, R., Holland, T., 1999. Relating formulations of the thermodynamics of mineral solid solutions: activity modeling of pyroxenes, amphiboles, and micas. Am. Mineral. 84, 1–14.

Raimbourg, H., Goffé, B., Jolivet, L., 2007. Garnet reequilibration and growth in the eclogite facies and geodynamical evolution near peak metamorphic conditions. Contrib. Mineral. Petrol. 153, 1–28. doi:10.1007/s00410-006-0130-3.

Rao, R.U.M., Rao, G.V., Narain, H., 1976. Radioactive heat generation and heat flow in the Indian shield. Earth Planet. Sci. Lett. 30, 57–64.

Rodriguez, E., Morris, C.S., Belz, J.E., Chapin, E.C., Martin, J.M., Daffer, W., Hensley, S., 2005. An assessment of the SRTM topographic products. Technical Report JPL D-31639. Jet Propulsion Laboratory, Pasadena, California. 143 pp.

Rubie, D.C., 1986. The catalysis of mineral reactions by water and restrictions on the presence of aqueous fluid during metamorphism. Mineral. Mag. 50, 399–415.

Rubie, D.C., 1998. Disequilibrium during metamorphism: the role of nucleation kinetics. In: Treloar, P.J., O, P., Brien (Eds.), What Drives Metamorphism and Metamorphic Reactions? Geol. Soc., London, Spec. Publ., vol. 138, pp. 199–214.

Rudnick, R.L., Fountain, D.M., 1995. Nature and composition of the continental crust — a lower crustal perspective. Rev. Geophys. 33 (3), 267–309.

Rudnick, R.L., Gao, S., 2003. The composition of the continental crust, in: Holland, H.D., Turekian, K.K. (Eds.) Treatise on Geochemistry, Vol. 3; The Crust (Ed. Rudnick, R.L.) pp. 1–64, Elsevier-Pergamon, Oxford.

Rushmer, T., 1991. Partial melting of two amphibolites: contrasting experimental results under fluid-absent conditions. Contrib. Mineral. Petrol. 107, 41–59.

Saul, J., Kumar, M.R., Sarkar, D., 2000. Lithospheric and upper mantle structure of the Indian Shield, from teleseismic receiver functions. Geophys. Res. Lett. 27 (16), 2356–2360.

Schulte-Pelkum, V., Monsalve, G., Sheehan, A., Pandey, M.R., Sapkota, S., Bilham, R., Wu, F., 2005. Imaging the Indian subcontinent beneath the Himalaya. Nature 435, 1222–1225.

Sun, W., 1989. Bouguer Gravity Anomaly Map of the People's Republic of China. Chin. Acad. Geoexploration, Beijing.

Szafián, P., Horváth, F., 2006. Crustal structure in the Carpatho–Pannonian region: insights from three-dimensional gravity modelling and their geodynamic significance. Int. J. Earth Sci. 95, 50–67.

Talwani, M., Worzel, J.I., Landisman, M., 1959. Rapid gravity computations for two-dimensional bodies with application to the Mendocino submarine fracture zone. J. Geophys. Res. 64, 46–59.

Tiwari, V.M., Vyghreswara, R., Mishra, D.C., Singh, B., 2006. Crustal structure across Sikkim, NE Himalaya from new gravity and magnetic data. Earth Planet. Sci. Lett. 247, 61–69.

Turcotte, D.L., Schubert, G., 1982. Geodynamics, Application of Continuum Physics to Geological Problems. John Wiley & Sons, New York. 450 pp.

Vance, D., O, Nions, R.K., 1992. Prograde and retrograde thermal histories from the central Swiss Alps. Earth Planet. Sci. Lett. 114, 113–129.

Vergne, J., Nábělek, J.L., Hi-CLIMB Team, 2005. Geometry and characteristics of the Main Himalayan Thrust in Nepal/Tibet revealed by the Hi-CLIMB seismological experiment. Eos Trans. AGU 86 (52) Fall Meet. Suppl., Abstract T52A-03.

Wei, C.J., Powell, R., 2003. Phase relations in high-pressure metapelites in the system KFMASH (K2O-FeO-MgO-Al2O3-SiO2-H2O) with application to natural rocks. Contrib. Mineral. Petrol. 145, 301–315.

Wessel, P., Smith, W.H.F., 1991. Free software helps map and display data. EoS Trans. AGU, 72, pp. 441 and 445–446.

White, R.W., Powell, R., Holland, T.J.B., Worley, B.A., 2000. The effect of TiO_2 and Fe_2O_3 on metapelitic assemblages at greenschist and amphibolite facies conditions: mineral equilibria calculations in the system K_2O–FeO–MgO–Al_2O_3–SiO_2–H_2O–TiO_2–Fe_2O_3. J. Metamorph. Geol. 18, 497–511.

White, R.W., Powell, R., Phillips, G.N., 2003. A mineral equilibria study of the hydrothermal alteration in mafic greenschist facies rocks at Kalgoorlie, Western Australia. J. Metamorph. Geol. 21, 455–468.

Won, I.J., Bevis, M., 1987. Computing the gravitational and magnetic anomalies due to a polygon: algorithms and Fortran subroutines. Geophysics 52 (2), 232–238.

Wood, B.J., Walther, J.W., 1983. Rates of hydrothermal reactions. Science 222, 413–415. doi:10.1126/science.222.4622.413.

Zhao, W., Nelson, K.D., Project INDEPTH Team, 1993. Deep seismic-reflection evidence continental underthrusting beneath Southern Tibet. Nature 366, 557–559.

Zhu, L., 2000. Crustal structure across the San Andreas Fault, Southern California from teleseismic converted waves. Earth Planet. Sci. Lett. 179, 183–190.

Zhu, L., Kanamori, H., 2000. Moho depth variation in Southern California from teleseismic receiver functions. J. Geophys. Res. 105, 2969–2980.

Zienkiewicz, O.C., Taylor, R.L., 1989. The Finite Element Method. McGraw-Hill, New York.